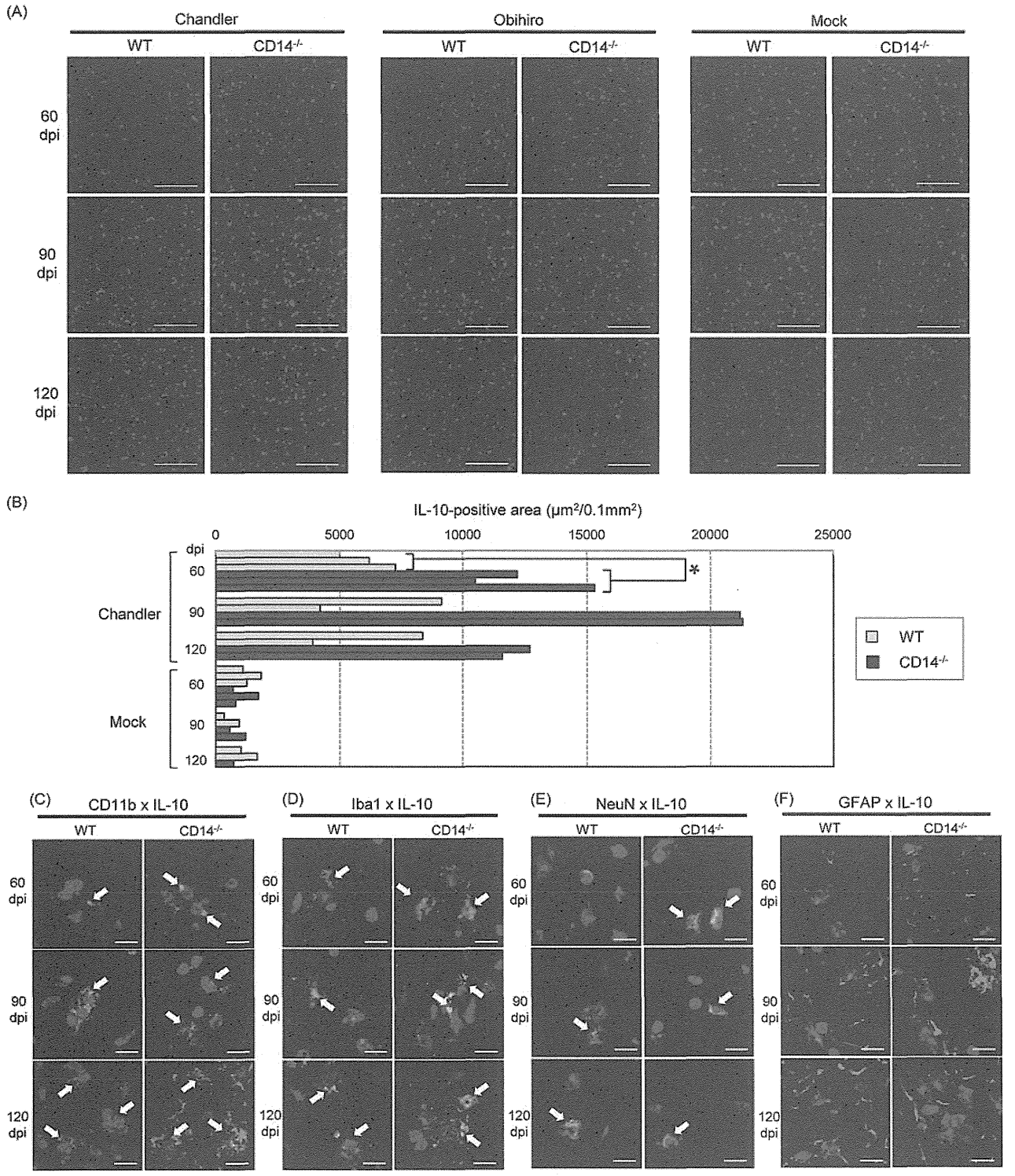

FIG 8 Expression of IL-10 in the brains of WT and CD14$^{-/-}$ mice infected with the Chandler and Obihiro strains. (A) Immunofluorescence staining of IL-10. Frozen blocks of the brains harvested at 60, 90, and 120 dpi were subjected to immunofluorescence staining. Representative images from the thalamus at each time point are shown. Bars, 50 μm. Red, IL-10; blue, nuclei. (B) Quantitative analysis of IL-10-positive areas in the thalamus of Chandler-infected mice. The areas positive for IL-10 (μm^2/0.1 mm^2) were quantified using Imaris ver 7.6.1 (Bitplane). The numbers of mice used for the analysis were 3 for both WT and CD14$^{-/-}$ mice at 60 dpi, 2 for both WT and CD 14$^{-/-}$ mice at 90 dpi, 2 for WT mice at 120 dpi, and 1 CD14$^{-/-}$ mouse at 120 dpi. *, $P < 0.01$, Student's t test. (C to F) Double immunofluorescence staining of IL-10 with CD11b (C), Iba1 (D), NeuN (E), and GFAP (F). Representative images from the thalamus of the Chandler-infected mice are shown. Green, immunoreactivities for these markers; red, IL-10; blue, nuclei. Arrows show double-positive cells. Bars, 10 μm.

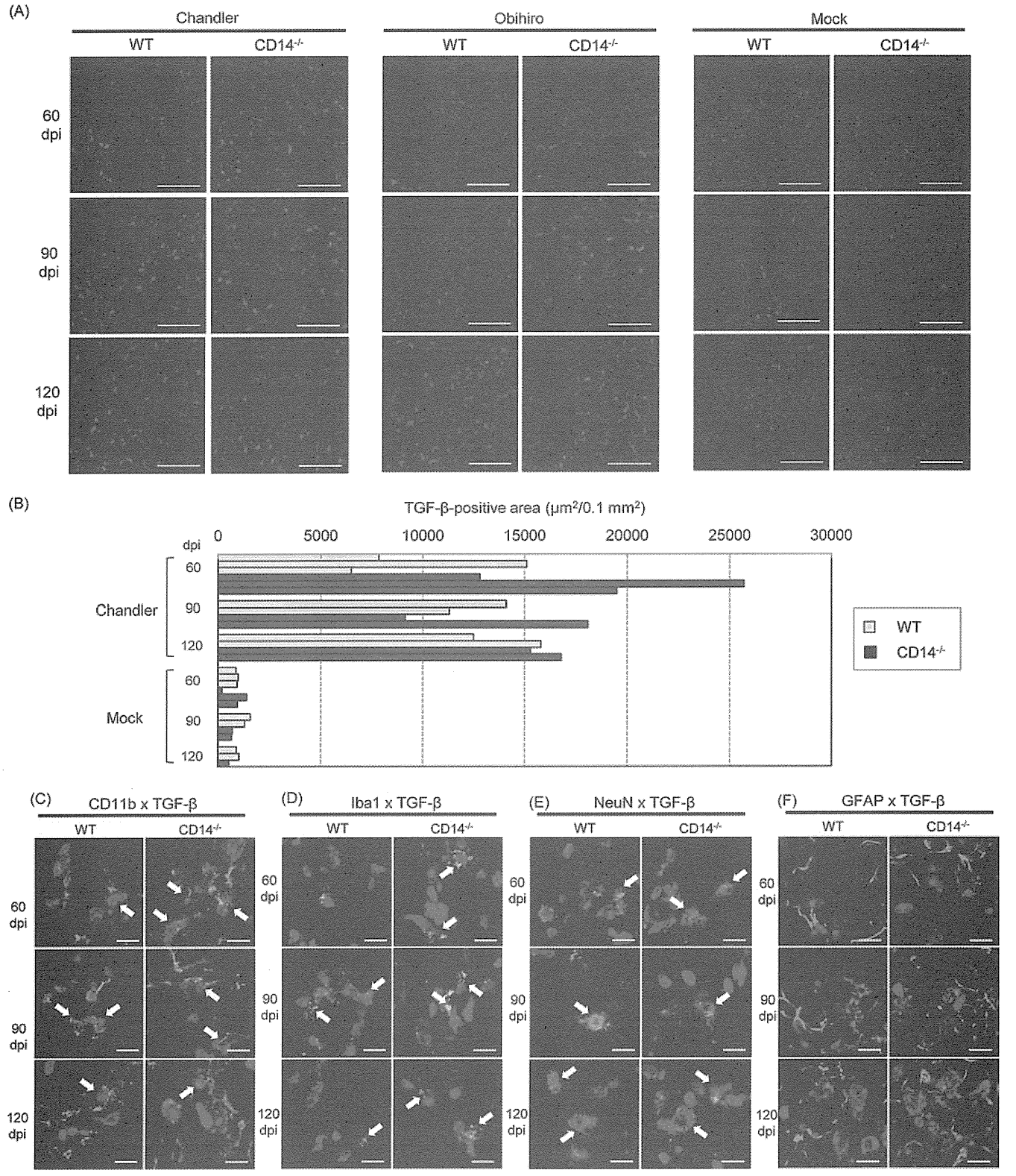

FIG 9 Expression of TGF-β in the brains of WT and CD14$^{-/-}$ mice infected with the Chandler and Obihiro strains. (A) Immunofluorescence staining of TGF-β at 60, 90, and 120 dpi. Representative images from the thalamus are shown for each time point. Bars, 50 μm. Red, TGF-β; blue, nuclei. (B) Quantitative analysis of TGF-β-positive areas in the thalamus of Chandler-infected mice. The method and mice used for the quantification are the same as in the legend for Fig. 8. (C to F) Double immunofluorescence staining of TGF-β with CD11b (C), Iba1 (D), NeuN (E), and GFAP (F). Representative figures from the thalamus of the Chandler-infected mice are shown. Green, immunoreactivities for these markers; red, TGF-β; blue, nuclei. Arrows show double-positive cells. Bars, 10 μm.

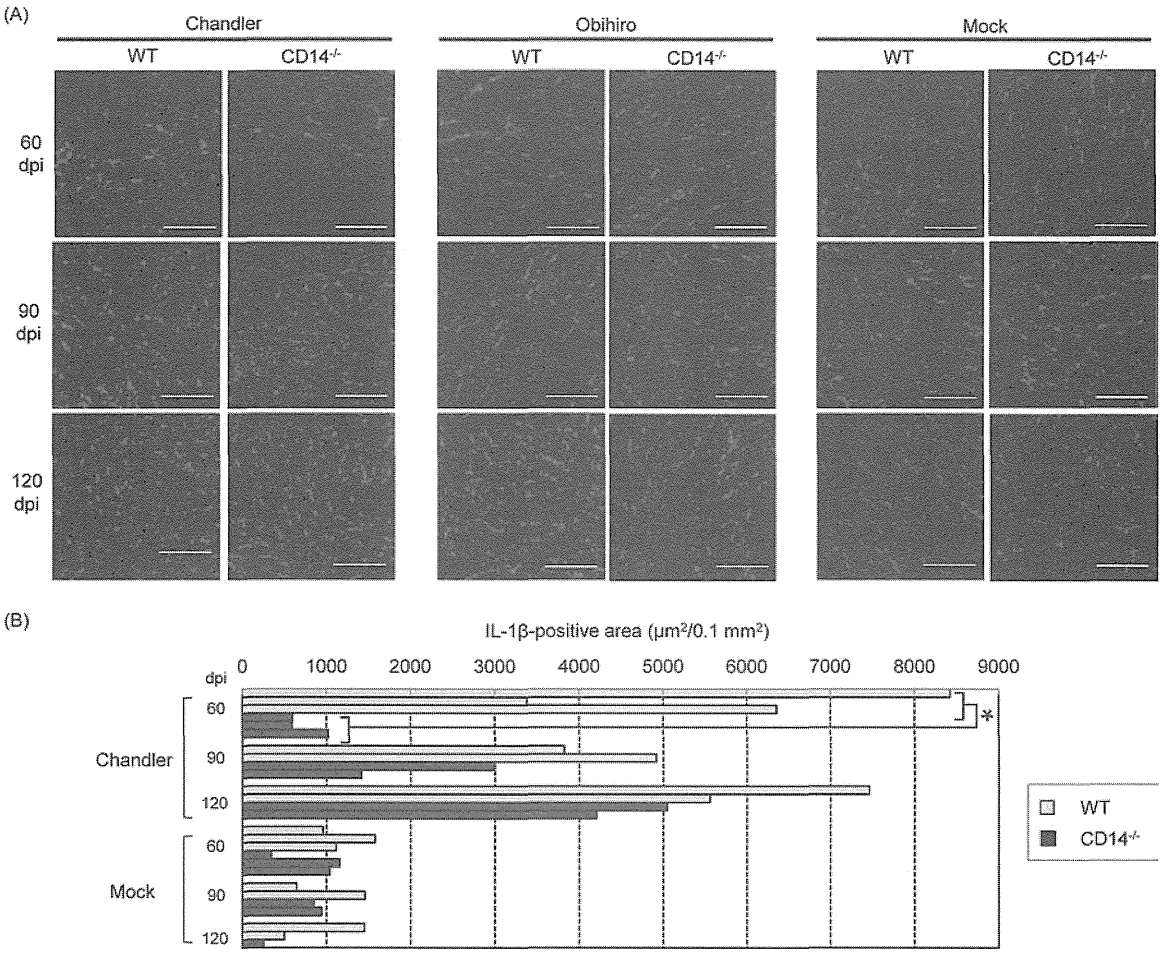

FIG 10 Expression of IL-1β in the brains of prion-infected WT and CD14$^{-/-}$ mice. (A) Immunofluorescence staining of IL-1β in the internal capsule of mice infected with Chandler or Obihiro strains at 60, 90, and 120 dpi. Bars, 50 μm; red, IL-1β; blue, nuclei. (B) Quantitative analysis of IL-1β-positive areas in the thalamus of Chandler-infected mice. The method and mice used for the quantification are the same as in the legend for Fig. 8. *, $P < 0.01$, Welch's *t* test.

Ablation of myeloid differentiation factor 88 (MyD88), an obligate signal transducer adaptor protein for TLRs, did not affect the neuropathology of prion diseases after intracerebral inoculation of prions, indicating that TLR signaling through MyD88, resulting in NF-κb activation, is not involved in prion neuropathogenesis (37). However, as TLRs can utilize both MyD88-dependent and -independent pathways (38), TLR2 also utilizes the Toll/interleukin 1 receptor domain containing adaptor protein (39). Thus, it would seem possible that CD14 can transduce cellular signaling through an association with TLRs other than TLR4 and MyD88-independent pathways and be able to modulate the inflammatory milieu, which may influence the pathogenesis of prion diseases.

In addition to reduced deposition of pathogenic agents, another similarity of CD14$^{-/-}$ mice in prion infection and the AD model is the upregulation of the anti-inflammatory cytokine IL-10 (17). This makes it conceivable that the phenotype of the microglia shifted to an anti-inflammatory, alternative activation status, even though the TNF-α gene expression was also more upregulated in the AD model mice with the CD14$^{-/-}$ background than in those with the WT background (17). Among anti-inflammatory cytokines, both IL-10 and TGF-β have been reported to be involved in the pathogenesis of prion diseases. Thackray et al. reported that survival times of IL-10-deficient mice was remarkably short (8), although the mouse genetic background greatly influences the effect of IL-10 on prion diseases (40), suggesting a significant suppressive role of this cytokine in the disease progression. Inhibition of TGF-β activity facilitated cerebral inflammation and acute neuronal death in ME7-infected mice (9). IL-10 has been reported to have a neuroprotective role by blocking caspase-3-like activity (41), and TGF-β also promotes neuronal survival by upregulating anti-apoptotic Bcl-2 family proteins (42). Therefore, an earlier expression of these anti-inflammatory cytokines may partially contribute to the prolonged survival of CD14$^{-/-}$ mice. Furthermore, both IL-10 and TGF-β provide anti-inflammatory effects by downregulating proinflammatory mediators such as IL-1β, IL-6, TNF-α, and NO (43–45). Indeed, expression of IL-1β in some brain regions of CD14$^{-/-}$ mice appeared to be lower than in WT mice (Fig. 10). However, it is also possible that the lower expression of IL-1β here resulted from a lack of TLR-CD14 signaling (46).

In AD model mice, bone marrow-derived microglia infiltrated from the peripheral circulation have protective potential against Aβ deposition and cognitive impairment in the early stage of the disease (47, 48), although it is controversial whether the protective

effect is due to a clearance of Aβ by microglia (49, 50). However, it is also possible that at a later stage, increased Aβ production may overwhelm the microglial activity, or the proinflammatory milieu may decrease the phagocytic activity of microglia (51), or microglia may change the activation status to a more proinflammatory and neurotoxic phenotype (52). PrP^{Sc} is believed to be produced in intracellular organelles such as early and recycling endosomes as well as on the plasma membrane (53–55). This would seem to exclude microglia from any role in the clearance of PrP^{Sc} itself by phagocytosis in the early stage of infection, although microglia remove neurons damaged by PrP^{Sc} accumulation (1, 56). Thus, the delayed PrP^{Sc} accumulation in the early stage of the disease in $CD14^{-/-}$ mice may imply the existence of a brain niche with accelerated microglial activation that may provide anti-prion propagation conditions, particularly at the early stage of the disease.

In this study, we showed that the increased activation of microglia accompanied by the altered expression of anti-inflammatory cytokines is possibly involved in the prolonged survival times and delayed deposition of PrP^{Sc} in prion-infected $CD14^{-/-}$ mice. This suggests that a CD14-dependent signaling pathway in microglia plays some role in the acceleration of the disease progression. Further analyses of the activation states of microglia and microglial functions would provide a better understanding of the roles of microglia in prion pathogenesis.

ACKNOWLEDGMENTS

This work was supported by a Grant-in-Aid for Science Research (A) (grant no. 23248050), a Grant for Challenging Exploratory Research (grant no. 23658233), a Grant-in-Aid for Young Researcher (B) (grant no. 23780303), and a grant from the global COE program (F-001) and a grant from the Program of Founding Research Centers for Emerging and Reemerging Infectious Diseases, from the Ministry of Education, Culture, Sports, Science, and Technology, Japan. This work was also supported by a grant for TSE research (H23-Shokuhin-Ippan-005) and a grant from the Research on Measures for Intractable Diseases program (grant no. H23-Nanchi-Ippan-013) from the Ministry of Health, Labor and Welfare of Japan. This work was also supported in part by a Grant-in-Aid from the BSE Control Project of the Ministry of Agriculture, Forestry and Fisheries of Japan.

We thank Zensho Co., Ltd., for use of the biosafety level 3 (BSL3) facility.

REFERENCES

1. **Williams A, Lucassen PJ, Ritchie D, Bruce M.** 1997. PrP deposition, microglial activation, and neuronal apoptosis in murine scrapie. Exp. Neurol. **144**:433–438.
2. **Giese A, Brown DR, Groschup MH, Feldmann C, Haist I, Kretzschmar HA.** 1998. Role of microglia in neuronal cell death in prion disease. Brain Pathol. **8**:449–457.
3. **Kettenmann H, Hanisch UK, Noda M, Verkhratsky A.** 2011. Physiology of microglia. Physiol. Rev. **91**:461–553.
4. **Ransohoff RM, Perry VH.** 2009. Microglial physiology: unique stimuli, specialized responses. Annu. Rev. Immunol. **27**:119–145.
5. **Block ML, Zecca L, Hong JS.** 2007. Microglia-mediated neurotoxicity: uncovering the molecular mechanisms. Nat. Rev. Neurosci. **8**:57–69.
6. **Neumann H, Kotter MR, Franklin RJ.** 2009. Debris clearance by microglia: an essential link between degeneration and regeneration. Brain **132**: 288–295.
7. **Schultz J, Schwarz A, Neidhold S, Burwinkel M, Riemer C, Simon D, Kopf M, Otto M, Baier M.** 2004. Role of interleukin-1 in prion disease-associated astrocyte activation. Am. J. Pathol. **165**:671–678.
8. Thackray AM, McKenzie AN, Klein MA, Lauder A, Bujdoso R. 2004. Accelerated prion disease in the absence of interleukin-10. J. Virol. **78**: 13697–13707.
9. **Boche D, Cunningham C, Docagne F, Scott H, Perry VH.** 2006. TGF-beta1 regulates the inflammatory response during chronic neurodegeneration. Neurobiol. Dis. **22**:638–650.
10. **Hwang D, Lee IY, Yoo H, Gehlenborg N, Cho JH, Petritis B, Baxter D, Pitstick R, Young R, Spicer D, Price ND, Hohmann JG, Dearmond SJ, Carlson GA, Hood LE.** 2009. A systems approach to prion disease. Mol. Syst. Biol. **5**:252. doi:10.1038/msb.2009.10.
11. **Xiang W, Windl O, Wunsch G, Dugas M, Kohlmann A, Dierkes N, Westner IM, Kretzschmar HA.** 2004. Identification of differentially expressed genes in scrapie-infected mouse brains by using global gene expression technology. J. Virol. **78**:11051–11060.
12. **Chow JC, Young DW, Golenbock DT, Christ WJ, Gusovsky F.** 1999. Toll-like receptor-4 mediates lipopolysaccharide-induced signal transduction. J. Biol. Chem. **274**:10689–10692.
13. **Kirschning CJ, Wesche H, Merrill Ayres T, Rothe M.** 1998. Human toll-like receptor 2 confers responsiveness to bacterial lipopolysaccharide. J. Exp. Med. **188**:2091–2097.
14. **Letiembre M, Liu Y, Walter S, Hao W, Pfander T, Wrede A, Schulz-Schaeffer W, Fassbender K.** 2009. Screening of innate immune receptors in neurodegenerative diseases: a similar pattern. Neurobiol. Aging **30**: 759–768.
15. **Baldini M, Lohman IC, Halonen M, Erickson RP, Holt PG, Martinez FD.** 1999. A Polymorphism* in the 5′ flanking region of the CD14 gene is associated with circulating soluble CD14 levels and with total serum immunoglobulin E. Am. J. Respir. Cell Mol. Biol. **20**:976–983.
16. **Lin JJ, Chen CH, Yueh KC, Chang CY, Lin SZ.** 2006. A CD14 monocyte receptor polymorphism and genetic susceptibility to Parkinson's disease for females. Parkinsonism Relat. Disord. **12**:9–13.
17. **Reed-Geaghan EG, Reed QW, Cramer PE, Landreth GE.** 2010. Deletion of CD14 attenuates Alzheimer's disease pathology by influencing the brain's inflammatory milieu. J. Neurosci. **30**:15369–15373.
18. **Kim CL, Umetani A, Matsui T, Ishiguro N, Shinagawa M, Horiuchi M.** 2004. Antigenic characterization of an abnormal isoform of prion protein using a new diverse panel of monoclonal antibodies. Virology **320**:40–51.
19. **Paxinos G, Franklin KBJ.** 2001. The mouse brain in stereotaxic coordinates, 2nd ed. Academic Press, San Diego, CA.
20. **Uryu M, Karino A, Kamihara Y, Horiuchi M.** 2007. Characterization of prion susceptibility in Neuro2a mouse neuroblastoma cell subclones. Microbiol. Immunol. **51**:661–669.
21. **Yamasaki T, Suzuki A, Shimizu T, Watarai M, Hasebe R, Horiuchi M.** 2012. Characterization of intracellular localization of PrP(Sc) in prion-infected cells using a mAb that recognizes the region consisting of aa 119-127 of mouse PrP. J. Gen. Virol. **93**:668–680.
22. **Song CH, Furuoka H, Kim CL, Ogino M, Suzuki A, Hasebe R, Horiuchi M.** 2008. Effect of intraventricular infusion of anti-prion protein monoclonal antibodies on disease progression in prion-infected mice. J. Gen. Virol. **89**:1533–1544.
23. **Pastrana MA, Sajnani G, Onisko B, Castilla J, Morales R, Soto C, Requena JR.** 2006. Isolation and characterization of a proteinase K-sensitive PrPSc fraction. Biochemistry **45**:15710–15717.
24. **Tzaban S, Friedlander G, Schonberger O, Horonchik L, Yedidia Y, Shaked G, Gabizon R, Taraboulos A.** 2002. Protease-sensitive scrapie prion protein in aggregates of heterogeneous sizes. Biochemistry **41**: 12868–12875.
25. **Fischer M, Rulicke T, Raeber A, Sailer A, Moser M, Oesch B, Brandner S, Aguzzi A, Weissmann C.** 1996. Prion protein (PrP) with amino-proximal deletions restoring susceptibility of PrP knockout mice to scrapie. EMBO J. **15**:1255–1264.
26. **Ford AL, Goodsall AL, Hickey WF, Sedgwick JD.** 1995. Normal adult ramified microglia separated from other central nervous system macrophages by flow cytometric sorting. Phenotypic differences defined and direct ex vivo antigen presentation to myelin basic protein-reactive CD4+ T cells compared. J. Immunol. **154**:4309–4321.
27. **Becher B, Antel JP.** 1996. Comparison of phenotypic and functional properties of immediately ex vivo and cultured human adult microglia. Glia **18**:1–10.
28. **Cosenza MA, Zhao ML, Si Q, Lee SC.** 2002. Human brain parenchymal microglia express CD14 and CD45 and are productively infected by HIV-1 in HIV-1 encephalitis. Brain Pathol. **12**:442–455.
29. **Cosenza-Nashat MA, Kim MO, Zhao ML, Suh HS, Lee SC.** 2006. CD45 isoform expression in microglia and inflammatory cells in HIV-1 encephalitis. Brain Pathol. **16**:256–265.
30. **Masliah E, Mallory M, Hansen L, Alford M, Albright T, Terry R, Shapiro P, Sundsmo M, Saitoh T.** 1991. Immunoreactivity of CD45, a

protein phosphotyrosine phosphatase, in Alzheimer's disease. Acta Neuropathol. 83:12–20.
31. Gomez-Nicola D, Fransen NL, Suzzi S, Perry VH. 2013. Regulation of microglial proliferation during chronic neurodegeneration. J. Neurosci. 33:2481–2493.
32. Burwinkel M, Schwarz A, Riemer C, Schultz J, van Landeghem F, Baier M. 2004. Rapid disease development in scrapie-infected mice deficient for CD40 ligand. EMBO Rep. 5:527–531.
33. Riemer C, Schultz J, Burwinkel M, Schwarz A, Mok SW, Gultner S, Bamme T, Norley S, van Landeghem F, Lu B, Gerard C, Baier M. 2008. Accelerated prion replication in, but prolonged survival times of, prion-infected CXCR3$^{-/-}$ mice. J. Virol. 82:12464–12471.
34. Priller J, Prinz M, Heikenwalder M, Zeller N, Schwarz P, Heppner FL, Aguzzi A. 2006. Early and rapid engraftment of bone marrow-derived microglia in scrapie. J. Neurosci. 26:11753–11762.
35. Spinner DS, Cho IS, Park SY, Kim JI, Meeker HC, Ye X, Lafauci G, Kerr DJ, Flory MJ, Kim BS, Kascsak RB, Wisniewski T, Levis WR, Schuller-Levis GB, Carp RI, Park E, Kascsak RJ. 2008. Accelerated prion disease pathogenesis in Toll-like receptor 4 signaling-mutant mice. J. Virol. 82: 10701–10708.
36. Henneke P, Takeuchi O, van Strijp JA, Guttormsen HK, Smith JA, Schromm AB, Espevik TA, Akira S, Nizet V, Kasper DL, Golenbock DT. 2001. Novel engagement of CD14 and multiple toll-like receptors by group B streptococci. J. Immunol. 167:7069–7076.
37. Prinz M, Heikenwalder M, Schwarz P, Takeda K, Akira S, Aguzzi A. 2003. Prion pathogenesis in the absence of Toll-like receptor signalling. EMBO Rep. 4:195–199.
38. Kawai T, Akira S. 2010. The role of pattern-recognition receptors in innate immunity: update on Toll-like receptors. Nat. Immunol. 11:373–384.
39. Kenny EF, Talbot S, Gong M, Golenbock DT, Bryant CE, O'Neill LA. 2009. MyD88 adaptor-like is not essential for TLR2 signaling and inhibits signaling by TLR3. J. Immunol. 183:3642–3651.
40. Tamguney G, Giles K, Glidden DV, Lessard P, Wille H, Tremblay P, Groth DF, Yehiely F, Korth C, Moore RC, Tatzelt J, Rubinstein E, Boucheix C, Yang X, Stanley P, Lisanti MP, Dwek RA, Rudd PM, Moskovitz J, Epstein CJ, Cruz TD, Kuziel WA, Maeda N, Sap J, Ashe KH, Carlson GA, Tesseur I, Wyss-Coray T, Mucke L, Weisgraber KH, Mahley RW, Cohen FE, Prusiner SB. 2008. Genes contributing to prion pathogenesis. J. Gen. Virol. 89:1777–1788.
41. Bachis A, Colangelo AM, Vicini S, Doe PP, De Bernardi MA, Brooker G, Mocchetti I. 2001. Interleukin-10 prevents glutamate-mediated cerebellar granule cell death by blocking caspase-3-like activity. J. Neurosci. 21:3104–3112.
42. Kim ES, Kim RS, Ren RF, Hawver DB, Flanders KC. 1998. Transforming growth factor-beta inhibits apoptosis induced by beta-amyloid peptide fragment 25-35 in cultured neuronal cells. Brain Res. Mol. Brain Res. 62:122–130.
43. Bogdan C, Nathan C. 1993. Modulation of macrophage function by transforming growth factor beta, interleukin-4, and interleukin-10. Ann. N. Y. Acad. Sci. 685:713–739.
44. Ledeboer A, Breve JJ, Poole S, Tilders FJ, Van Dam AM. 2000. Interleukin-10, interleukin-4, and transforming growth factor-beta differentially regulate lipopolysaccharide-induced production of pro-inflammatory cytokines and nitric oxide in co-cultures of rat astroglial and microglial cells. Glia 30:134–142.
45. Seyler I, Appel M, Devissaguet JP, Legrand P, Barratt G. 1997. Modulation of nitric oxide production in RAW 264.7 cells by transforming growth factor-beta and interleukin-10: differential effects on free and encapsulated immunomodulator. J. Leukoc. Biol. 62:374–380.
46. Fitzgerald KA, Rowe DC, Golenbock DT. 2004. Endotoxin recognition and signal transduction by the TLR4/MD2-complex. Microbes Infect. 6:1361–1367.
47. El Khoury J, Toft M, Hickman SE, Means TK, Terada K, Geula C, Luster AD. 2007. Ccr2 deficiency impairs microglial accumulation and accelerates progression of Alzheimer-like disease. Nat. Med. 13:432–438.
48. Simard AR, Soulet D, Gowing G, Julien JP, Rivest S. 2006. Bone marrow-derived microglia play a critical role in restricting senile plaque formation in Alzheimer's disease. Neuron 49:489–502.
49. Grathwohl SA, Kalin RE, Bolmont T, Prokop S, Winkelmann G, Kaeser SA, Odenthal J, Radde R, Eldh T, Gandy S, Aguzzi A, Staufenbiel M, Mathews PM, Wolburg H, Heppner FL, Jucker M. 2009. Formation and maintenance of Alzheimer's disease beta-amyloid plaques in the absence of microglia. Nat. Neurosci. 12:1361–1363.
50. Mildner A, Schlevogt B, Kierdorf K, Bottcher C, Erny D, Kummer MP, Quinn M, Bruck W, Bechmann I, Heneka MT, Priller J, Prinz M. 2011. Distinct and non-redundant roles of microglia and myeloid subsets in mouse models of Alzheimer's disease. J. Neurosci. 31:11159–11171.
51. Koenigsknecht-Talboo J, Landreth GE. 2005. Microglial phagocytosis induced by fibrillar beta-amyloid and IgGs are differentially regulated by proinflammatory cytokines. J. Neurosci. 25:8240–8249.
52. Jimenez S, Baglietto-Vargas D, Caballero C, Moreno-Gonzalez I, Torres M, Sanchez-Varo R, Ruano D, Vizuete M, Gutierrez A, Vitorica J. 2008. Inflammatory response in the hippocampus of PS1M146L/APP751SL mouse model of Alzheimer's disease: age-dependent switch in the microglial phenotype from alternative to classic. J. Neurosci. 28:11650–11661.
53. Godsave SF, Wille H, Pierson J, Prusiner SB, Peters PJ. 2013. Plasma membrane invaginations containing clusters of full-length PrP(Sc) are an early form of prion-associated neuropathology in vivo. Neurobiol. Aging 34:1621–1631.
54. Godsave SF, Wille H, Kujala P, Latawiec D, DeArmond SJ, Serban A, Prusiner SB, Peters PJ. 2008. Cryo-immunogold electron microscopy for prions: toward identification of a conversion site. J. Neurosci. 28:12489–12499.
55. Jeffrey M, Goodsir CM, Bruce ME, McBride PA, Scott JR, Halliday WG. 1992. Infection specific prion protein (PrP) accumulates on neuronal plasmalemma in scrapie infected mice. Neurosci. Lett. 147:106–109.
56. Hughes MM, Field RH, Perry VH, Murray CL, Cunningham C. 2010. Microglia in the degenerating brain are capable of phagocytosis of beads and of apoptotic cells, but do not efficiently remove PrPSc, even upon LPS stimulation. Glia 58:2017–2030.

nature COMMUNICATIONS

ARTICLE

Received 24 Sep 2012 | Accepted 16 Apr 2013 | Published 14 May 2013

DOI: 10.1038/ncomms2873

Prions disturb post-Golgi trafficking of membrane proteins

Keiji Uchiyama[1], Naomi Muramatsu[1], Masashi Yano[1], Takeshi Usui[1,2], Hironori Miyata[3] & Suehiro Sakaguchi[1]

Conformational conversion of normal cellular prion protein PrP^{C} into pathogenic PrP^{Sc} is central to the pathogenesis of prion diseases. However, the pathogenic mechanism remains unknown. Here we show that post-Golgi vesicular trafficking is significantly delayed in prion-infected N2a cells. Accordingly, cell surface expression of membrane proteins examined, including PrP^{C}, insulin receptor involved in neuroprotection, and attractin, whose mutation causes prion disease-like spongiform neurodegeneration, is reduced. Instead, they accumulate in the Golgi apparatus. PrP^{Sc} is detected throughout endosomal compartments, being particularly abundant in recycling endosome. We also show reduced surface expression of PrP^{C} and insulin receptor in prion-infected mouse brains well before the onset of disease. These results suggest that prion infection might impair post-Golgi trafficking of membrane proteins to the cell surface in neurons via PrP^{Sc} accumulated in recycling endosome, and eventually induce neuronal dysfunctions associated with prion diseases.

[1] Division of Molecular Neurobiology, The Institute for Enzyme Research (KOSOKEN), The University of Tokushima, 3-18-15 Kuramoto, Tokushima 770-8503, Japan. [2] Student Laboratory, Faculty of Medicine, The University of Tokushima, 3-18-15 Kuramoto, Tokushima 770-8503, Japan. [3] Animal Research Center, University of Occupational and Environmental Health, 1-1 Iseigaoka, Yahatanishi, Kitakyushu 807-8555, Japan. Correspondence and requests for materials should be addressed to S.S. (email: sakaguch@ier.tokushima-u.ac.jp).

The normal cellular prion protein, PrP^C, is a glycosylphosphatidylinositol (GPI)-anchored membrane glycoprotein expressed most abundantly in neurons[1]. Conformational conversion of PrP^C into the abnormally folded, relatively proteinase K (PK)-resistant PrP^{Sc} has a pivotal role in prion diseases such as Creutzfeldt-Jakob disease and scrapie[1]. Mice devoid of PrP^C ($Prnp^{0/0}$) are resistant to prion disease even after intracerebral inoculation with prions[2–5]. However, the pathogenic mechanism of the diseases is unknown.

The Golgi apparatus is a specialized cytoplasmic organelle near the nucleus that sorts membrane and luminal proteins via vesicle transport from the endoplasmic reticulum (ER) to lysosomes, secretory vesicles and the cell surface. In neurons, it is involved in the axonal transport of proteins, and functional damage to it could have significant implications. Indeed, the Golgi apparatus might have a role in various neurodegenerative disorders, including Alzheimer's disease, Parkinson's disease and amyotrophic lateral sclerosis[6,7].

Reports suggest involvement of the Golgi apparatus in prion diseases. PrP^{Sc} has been detected near the Golgi apparatus in prion-infected cells[8]. Transgenic (tg) mice expressing PrP fused with green fluorescent protein on the wild-type background, that is, tg(PrP-EGFP)/$Prnp^{+/+}$ mice, developed prion disease after intracerebral inoculation with RML prions, with progressive accumulation of PrP-EGFP in the Golgi apparatus of neurons from the early stages of the infection[9]. The transmembrane form of PrP, ^{Ctm}PrP, with the N terminus in the cytosol and C terminus in the ER lumen is neurotoxic, causing prion disease-like neurodegeneration in mice[10,11]. Tg mice expressing a ^{Ctm}PrP-favouring mutant accumulated ^{Ctm}PrP at the Golgi apparatus in neurons[12,13].

Insulin signalling may regulate a neuroprotective function, synaptic plasticity and memory formation[14–21]. Loss-of-function for attractin causes prion disease-like spongiform neurodegeneration in animals[22]. However, the role of the insulin receptor (IR) and attractin in prion diseases is unknown.

In the present study, we show that post-Golgi vesicular trafficking is delayed in mouse neuroblastoma N2a cells persistently infected with scrapie prions. PrP^C cell surface expression diminishes and instead accumulates in the Golgi apparatus. Most PrP^{Sc} is in endosomal compartments, being particularly abundant in recycling endosomes. We also show that cell surface IR and attractin are reduced in infected cells, and downstream signalling of the IR is disturbed. Furthermore, cell surface PrP^C and IR are reduced in prion-infected mouse brains well before the onset of clinical symptoms. Another GPI-anchored membrane molecule, Thy-1, also reduces surface expression in infected brains. However, the glutamate receptor subunits GluR3 and NR1 are not affected. These results suggest that prion infection could impair post-Golgi vesicle transportation of some membrane proteins, including PrP^C, Thy-1, IR and attractin, to the cell surface by accumulating PrP^{Sc} in recycling endosomes eventually causing neuronal dysfunction.

Results

Post-Golgi trafficking is delayed in prion-infected cells. Uninfected N2aC24 line is a cloned N2a line overexpressesing exogenously transfected mouse PrP^C (ref. 23). Infected N2aC24L1-3 line is a clone of N2aC24 cells that were infected with 22L prions[23]. PrP^{Sc} was detectable in infected N2aC24L1-3 cells on western blotting (WB) (Fig. 1a). Cured N2aC24L1-3 cells were established in this study. Prion infection was cured by treatment with SAF32 anti-PrP antibody (Ab) against the octapeptide repeat region. Cured N2aC24L1-3 cells lack PrP^{Sc} (Fig. 1a). The Golgi apparatus is important for vesicular trafficking of membrane and secretory molecules. To assess the vesicular trafficking in these cells, we performed a vesicular transport assay with a temperature-sensitive mutant of the vesicular stomatitis virus-G protein fused with green fluorescent protein (GFP), designated VSV-G(ts045)–GFP. VSV-G(ts045)–GFP folds improperly at the non-permissive temperature of 39.5 °C, thereby remaining in the ER. In contrast, at the permissive temperature of 32 °C, the protein is properly folded and exits from the ER to the Golgi apparatus and then to the cell surface.

To assess prion infection on the transport of VSV-G(ts045)–GFP, uninfected N2aC24, infected N2aC24L1-3 and cured N2aC24L1-3 cells were transiently transfected with the VSV-G(ts045)–GFP expression vector at 39.5 °C and, 16 h after transfection, cultured at 32 °C with the protein synthesis inhibitor cycloheximide allowing monitoring of the already synthesized VSV-G(ts045)–GFP alone. The cells were fixed at various time points immediately after the culture was started at 32 °C and stained with Abs against GFP and the Golgi marker GM130 by immunohistochemistry (IHC). The fluorescent intensities of VSV-G(ts045)–GFP in the whole cell and the GM130-positive area were measured. About 10% of total VSV-G(ts045)–GFP was detected at the GM130-positive area in these cells at 0 min at 32 °C (Fig. 1b; Supplementary Fig. S1). This might be because a small portion of VSV-G(ts045)–GFP in the ER overlaps with the Golgi apparatus or is resistant to the non-permissive temperature, exiting from the ER to the Golgi apparatus, or both. As soon as the culture was started at 32 °C, VSV-G(ts045)–GFP began to accumulate in the Golgi apparatus with similar kinetics in the cells, reaching maximum at 30 min (Fig. 1b; Supplementary Fig. S1), indicating that vesicular trafficking of VSV-G(ts045)–GFP from the ER to the Golgi apparatus was not affected by prion infection. However, after 30 min at 32 °C, infected cells showed significantly delayed decreased VSV-G(ts045)–GFP fluorescent intensities in the Golgi apparatus, compared with uninfected cells (Fig. 1b; Supplementary Fig. S1). This delayed decrease was rescued in cured cells (Fig. 1b;. Supplementary Fig. S1). Similar delayed decrease in the fluorescent intensities of VSV-G(ts045)–GFP in the Golgi apparatus was observed in N2aC24Chm cells, N2aC24 cells persistently infected with Chandler prions (Fig. 1a,c). This delayed decrease was also recovered in cured N2aC24Chm cells (Fig. 1a,c). These results indicate that post-Golgi trafficking of VSV-G(ts045)–GFP was delayed in infected cells.

We further investigated the levels of VSV-G(ts045)–GFP transported to the cell surface using fluorescence-activated cell sorter (FACS) analysis. The transfected cells were cultured for 120 min at 32 °C with cycloheximide and then immediately subjected to FACS analysis. The cells expressing VSV-G(ts045)–GFP were detected by the GFP fluorescence, and VSV-G(ts045)–GFP transported to the cell surface were detected with anti-VSV-G Ab and DyLight 649-conjugated Ab (Supplementary Fig. S2a,b). The fluorescent signal corresponding to the surface VSV-G(ts045)–GFP was significantly lower in infected cells than in uninfected or cured cells (Supplementary Fig. S2a,b), indicating that VSV-G(ts045)–GFP transport was delayed to the cell surface in infected cells.

Impaired post-Golgi transport of PrP^C in infected cells. We investigated whether the post-Golgi trafficking of PrP^C to the cell surface might be impaired in infected cells. We first semi-quantified PrP^C expressed on the surface of uninfected N2aC24, infected N2aC24L1-3 and cured N2aC24L1-3 cells using biotin labelling of cell surface proteins. The labelled proteins were purified by avidin beads and subjected to WB with 6D11 anti-PrP Ab against an epitope within residues 93–109. Total PrP was

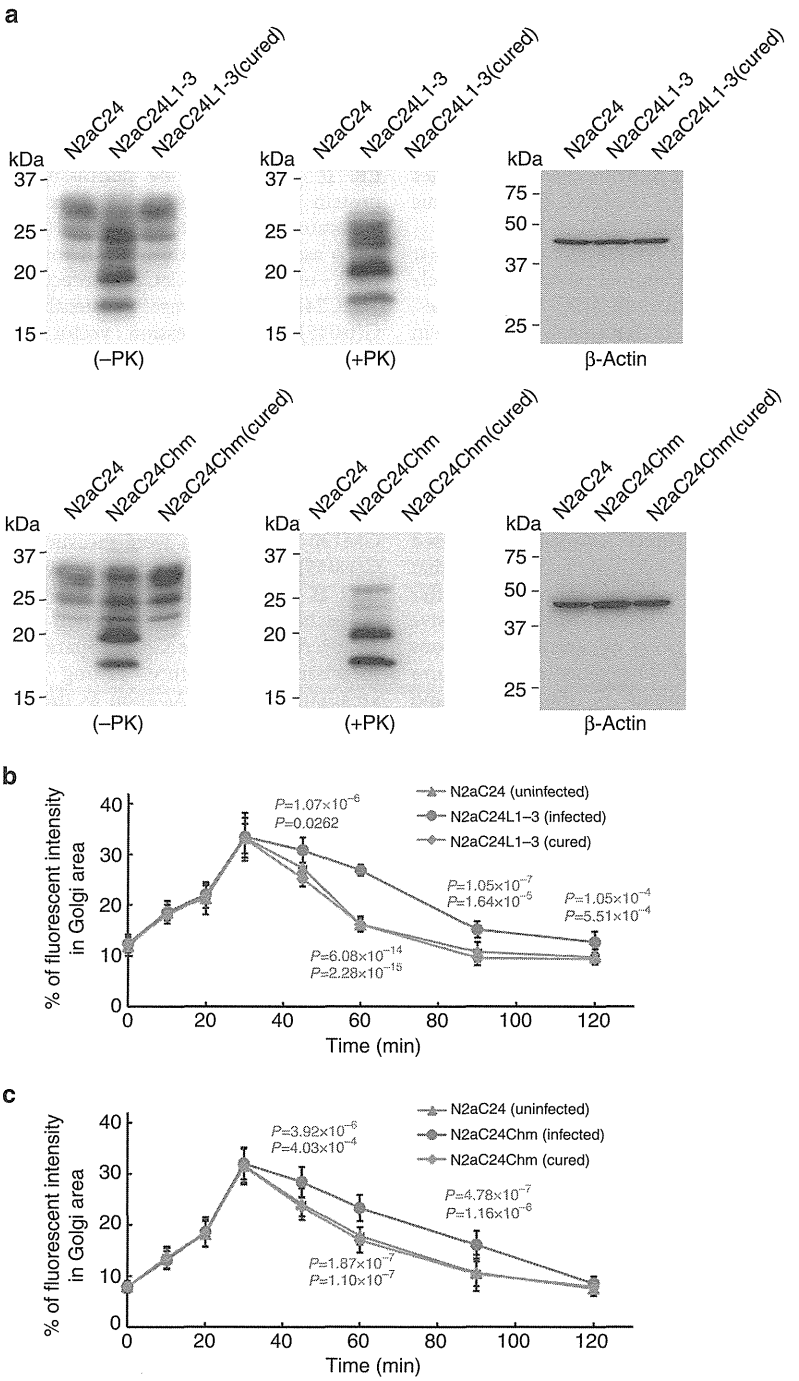

Figure 1 | Post-Golgi vesicular trafficking is delayed in 22L prion-infected N2aC24L1-3 and Chandler prion-infected N2aC24Chm cells. (**a**) Upper panels: WB of uninfected N2aC24, infected N2aC24L1-3 and cured N2aC24L1-3 cells with 6D11 anti-PrP Ab. Lower panels: WB of uninfected N2aC24, infected N2aC24Chm and cured N2aC24Chm cells with 6D11 anti-PrP Ab. PrP^{Sc} was detected in infected N2aC24L1-3 or N2aC24Chm cells, but not in uninfected N2aC24, cured N2aC24L1-3, and cured N2aC24Chm cells. Each cell lysate was treated without (−) or with (+) PK. β-Actin is an internal control. (**b**) Transport assay of VSV-G(ts045)-GFP in uninfected N2aC24, infected N2aC24L1-3 and cured N2aC24L1-3 cells. (**c**) Transport assay of VSV-G(ts045)-GFP in uninfected N2aC24, infected N2aC24Chm and cured N2aC24Chm cells. Cells were transfected with the vector encoding VSV-G(ts045)-GFP and incubated at the non-permissive temperature at 39.5 °C. Fluorescent intensities for VSV-G(ts045)-GFP at the Golgi region against those in the whole cell were determined in the randomly selected transfected cells ($n=14$–16) at various times, after the cells were transferred to the permissive temperature of 32 °C. Trafficking of VSV-G(ts045)-GFP in the cells was assessed as the kinetics of the protein in the Golgi area. The kinetics was defined as a change in the ratio of the fluorescent intensities of VSV-G(ts045)-GFP in the Golgi area to those in the whole cell over time. Post-Golgi trafficking of VSV-G(ts045) was significantly delayed in infected N2aC24L1-3 and N2aC24Chm cells, compared with that in uninfected N2aC24 cells. Blue and green *P*-values indicate significances of infected cells against those of uninfected or cured cells, respectively. No significant difference in the VSV-G(ts045)-GFP trafficking was observed between uninfected N2aC24 and cured N2aC24L1-3 or cured N2aC24Chm cells. Data were analysed using the Student's *t*-test.

increased because of the accumulation of PrP^{Sc} in infected cells (Fig. 2a,b). However, the biotinylated PrP levels were lower in infected cells, compared with uninfected cells (Fig. 2a,b). Reduced levels were recovered in cured cells (Fig. 2a,b). Less than 1% of the biotinylated PrP from infected cells were PK resistant (Fig. 2c), indicating that most of the biotinylated PrP are PrP^{C}. These results indicate that surface PrP^{C} is reduced in prion-infected cells.

We performed IHC of these cells using SAF83 anti-PrP Ab against an epitope within residues 126–164 under standard conditions of fixation and permeabilization, in which most PrP^{Sc} escapes labelling by the Ab. Hence, PrP^{C} is preferentially visualized. Consistent with PrP^{C} being a membrane glycoprotein, uninfected cells exhibited strong cell surface signals (Fig. 3a). However, in infected cells, a region near the nucleus, detected by anti-lamin A Ab, was aberrantly stained (Fig. 3a). The cell surface signals were still detectable but decreased in infected cells (Fig. 3a). The aberrant staining near the nucleus was absent in cured cells (Fig. 3a). We also costained infected cells with Abs against various organelle markers. Most of the SAF83-positive signals were costained with the Golgi markers, more strongly with the *trans*-Golgi network marker TGN38 than with the *cis*-Golgi marker giantin (Fig. 3b). Not all of the SAF83-positive signals were precisely costained with the *trans*-Golgi markers. The *trans*-Golgi network consists of distinct subcompartments[24]. Therefore, PrP^{C} might be preferentially accumulated in a specific *trans*-Golgi network subcompartment(s). A small proportion of the signals were stained with the recycling endosome markers, Rab11

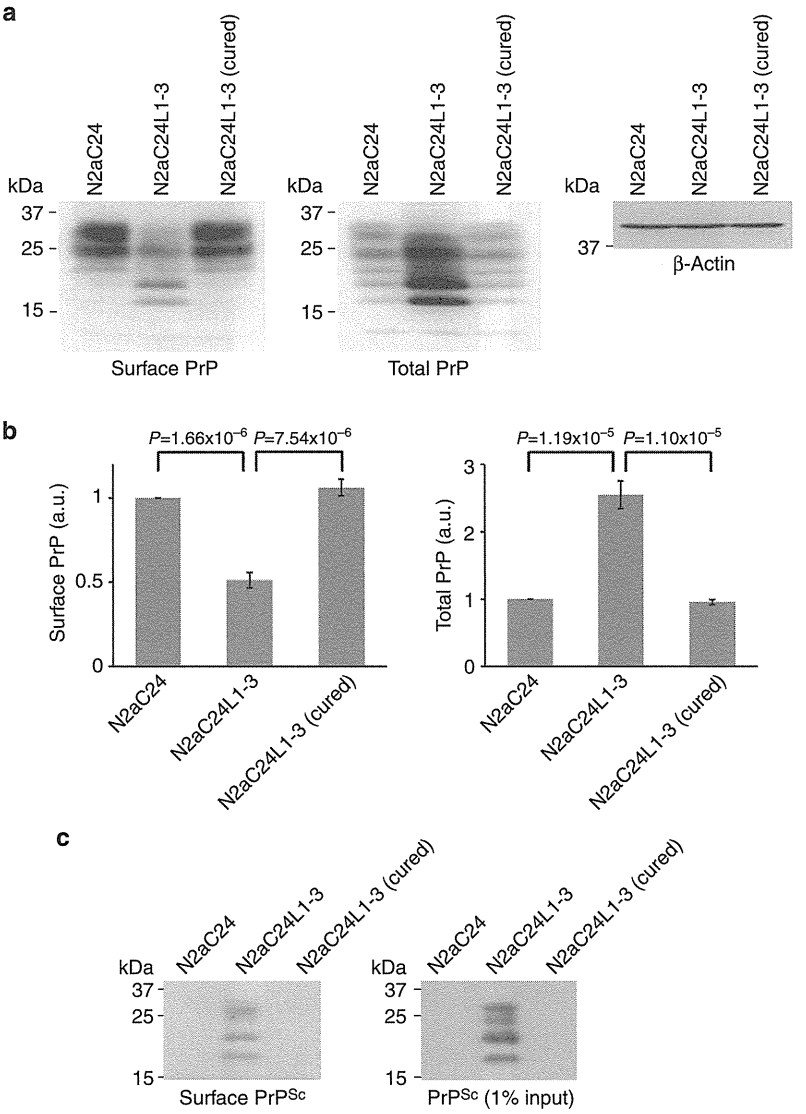

Figure 2 | Cell surface expression of PrP^{C} is decreased in infected cells. (**a**) WB with 6D11 anti-PrP Ab of biotin-labelled surface PrP and total PrP in uninfected N2aC24, infected N2aC24L1-3 and cured N2aC24L1-3 cells. Surface expression of PrP was reduced in infected N2aC24L1-3 cells, compared with that in uninfected N2aC24 and cured N2aC24L1-3 cells (left panel). Total PrP were increased in infected N2aC24L1-3 cells, due to accumulation of PrP^{Sc} (middle panel). β-Actin is an internal control (right panel). (**b**) Signal densities for PrP in each lane against those for β-actin were statistically analysed from three independent experiments using the Student's *t*-test. Vertical axes are indicated as an arbitrary unit (a.u.). Error bars, s.d. (**c**) WB of the purified and unpurified biotinylated PrP after PK treatment. Less than 1% of the biotinylated PrP from infected N2aC24L1-3 cells were PK resistant, indicating most biotinylated PrP are PrP^{C}.

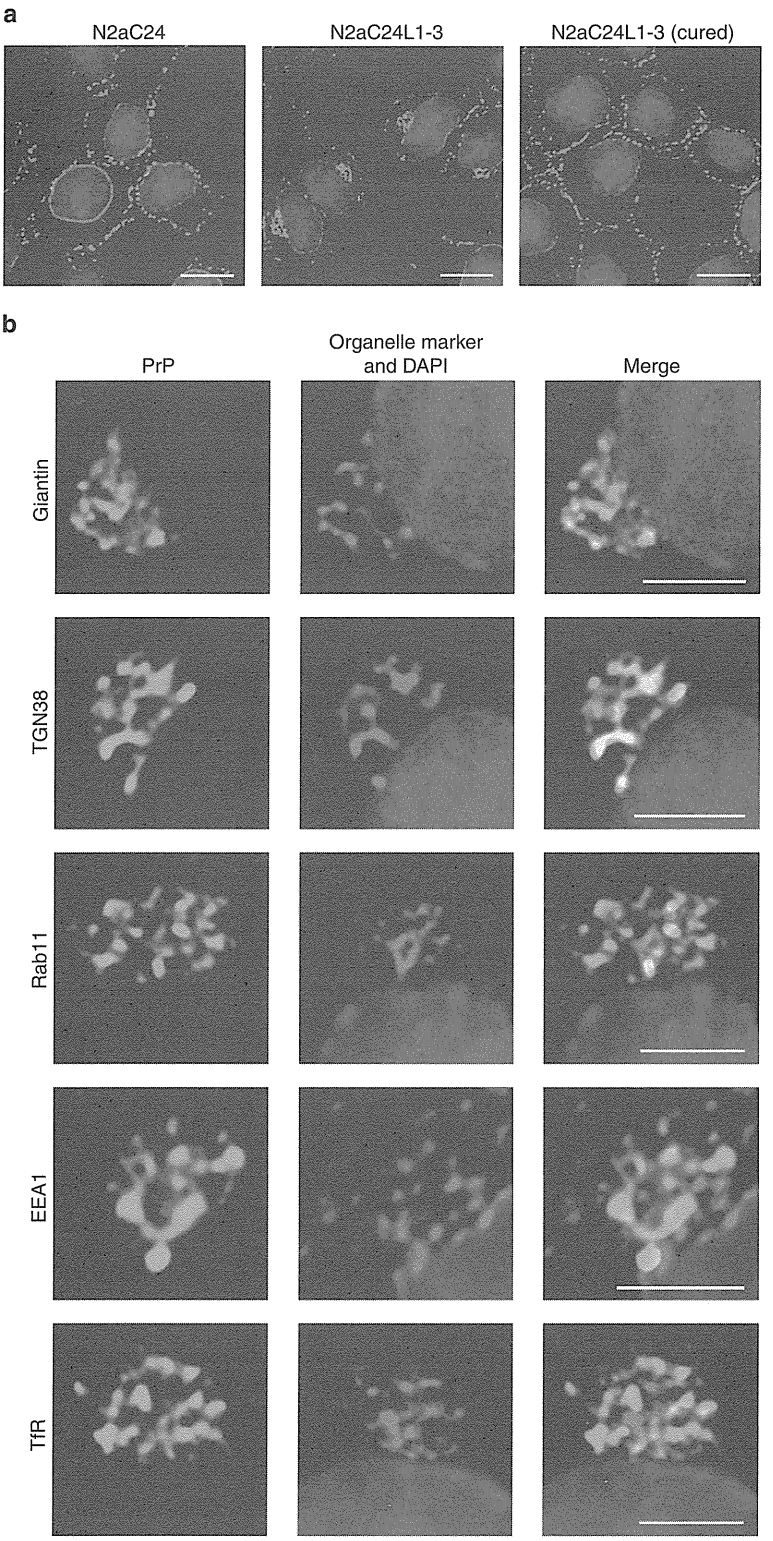

Figure 3 | Aberrant accumulation of PrP^C in the Golgi apparatus in infected cells. (**a**) Uninfected N2aC24, infected N2aC24L1-3 and cured N2aC24L1-3 cells were immunohistochemically stained with SAF83 anti-PrP Ab (green). Most signals were observed on the cell surface in uninfected N2aC24 and cured N2aC24L1-3 cells. In contrast, the surface signal was reduced and a region near the nucleus became stained in infected N2aC24L1-3 cells. The nuclear envelope was stained with anti-lamin A Ab (red). The nucleus was stained with DAPI (blue). (**b**) Costaining of PrP^C in infected N2aC24L1-3 cells with the *cis*-Golgi marker giantin, the *trans*-Golgi network marker TGN38, the recycling endosome markers Rab11 and TfR, and the early endosome marker EEA1. The PrP signal in the region near the nucleus was preferentially costained with the Golgi markers, particularly with the *trans*-Golgi network marker, TGN38, in infected N2aC24L1-3 cells. Green fluorescence, PrP; blue fluorescence, nucleus; red fluorescence, the organelle markers; yellow fluorescence, combined signals. Scale bars 5 μm.